OPEN

All-optical control of ultrafast photocurrents in unbiased graphene

Petr A. Obraztsov[1,2], Tommi Kaplas[2], Sergey V. Garnov[1], Makoto Kuwata-Gonokami[3], Alexander N. Obraztsov[4,2] & Yuri P. Svirko[2]

Correspondence and
requests for materials
should be addressed to
P.A.O. (petr.
obraztsov@uef.fi)

[1]A.M. Prokhorov General Physics Institute, Moscow, Russia, [2]Institute of Photonics, University of Eastern Finland, Joensuu, Finland, [3]Department of Physics, Graduate School of Science and Photon Science Center, The University of Tokyo, Tokyo, Japan, [4]Department of Physics, M.V. Lomonosov Moscow State University, Moscow, Russia.

Graphene has recently become a unique playground for studying light-matter interaction effects in low-dimensional electronic systems. Being of strong fundamental importance, these effects also open a wide range of opportunities in photonics and optoelectronics. In particular, strong and broadband light absorption in graphene allows one to achieve high carrier densities essential for observation of nonlinear optical phenomena. Here, we make use of strong photon-drag effect to generate and optically manipulate ultrafast photocurrents in graphene at room temperature. In contrast to the recent reports on injection of photocurrents in graphene due to external or built-in electric field effects and by quantum interference, we force the massless charge carriers to move via direct transfer of linear momentum from photons of incident laser beam to excited electrons in unbiased sample. Direction and amplitude of the drag-current induced in graphene are determined by polarization, incidence angle and intensity of the obliquely incident laser beam. We also demonstrate that the irradiation of graphene with two laser beams of the same wavelength offers an opportunity to manipulate the photocurrents in time domain. The obtained all-optical control of the photocurrents opens new routes towards graphene based high-speed and broadband optoelectronic devices.

Owing to a gapless linear band structure and a high mobility of massless charge carriers, graphene is widely recognized as a material of future all-wavelength optoelectronics[1–3]. There were proposed several ways to utilize photoexcited carriers. For example one can employ a built-in potential at the metal-graphene or graphene-graphene interfaces[4–6] or to apply external voltage. Another approach to study photoexcited carriers suggests injection and coherent control of ballistic photocurrents using quantum interference of one- and two-photon absorption pathways or frequency mixing[7–10]. Despite a strong third-order nonlinearity of graphene[11] observation of these effects requires high light intensities and perfect coherence of the interacting beams.

The photon drag effect (PDE)[12–14] offers an alternative all-optical way to generate and control the photocurrents in unbiased graphene. This second-order nonlinear optical phenomenon enables generation of the transient currents in a medium using a single linearly polarized obliquely incident laser beam. We demonstrate that the induced drag-currents can be manipulated in time domain by the second excitation beam at the same frequency which is not necessarily coherent with the first one. The directions, amplitudes and the temporal behavior of the induced currents are determined by intensities, mutual orientation and polarizations of the excitation beams.

The properties of the second-order nonlinear optical response are determined by the symmetry of a medium. Since graphene possesses the inversion centre, the second-order electric-dipole susceptibility of graphene is zero and generation of a direct current (DC) (photogalvanic effect) or DC polarization (optical rectification) is forbidden[15]. This restriction imposed by the centrosymmetricity of graphene can be lifted off by external or built-in electric field[16,17]. In free-standing pristine graphene, the nonlinear optical effects of the second order in the light field are only possible due to mechanisms that take into account a finite momentum that photon transfers to the electron. This transferred momentum results, in particular, to the PDE[12–14]. The PDE originates from the transfer of the absorbed photon momentum to a free carrier and is allowed in all materials, whether they process inversion symmetry or not. However, the energy and momentum conservation imply that momentum transfer from photon to electron (hole) requires participation of the lattice via the electron-phonon interaction. Since $ka \ll 1$, where k is the wave vector and a is the lattice parameter, the photon-drag current in most materials is negligibly weak. From the other hand the acquired momentum and, hence, the drag current survives for only the momentum relaxation time τ_p, which is also determined by the interaction between carriers and phonons. That is, the stronger the electron-phonon coupling, the higher the momentum transfer rate and the shorter the momentum relaxation time. The high carrier mobility, the linear energy dispersion and a relatively low (in

comparison with semiconductor crystals) momentum relaxation rates makes the PDE in graphene and graphene-based materials observable. We have previously demonstrated that in carbon nanotubes[18] and nanographite thin films[19,20] irradiated by nanosecond optical pulses at oblique incidence, the PDE gives rise to the strong DC current. Also, the significant contribution of the PDE to generation of the electron and spin currents in topological insulators[21] and graphene[22–24] was recently reported. However the latter works were mainly focused on the effects of photon helicity under intraband excitation in the far IR or THz range. Here, we show for the first time that interband excitation of graphene with linearly polarized visible or near IR light enables PDE, which leads to an efficient generation of the ultrafast in-plane current and THz generation.

Results

In the experiments, we used single- and multi-layered(ML) graphene samples, obtained by a chemical vapor deposition (CVD), with area of about 1 cm² and thicknesses ranging from 1 to approximately 40 atomic layers[25,26] deposited on dielectric (either SiO_2 or polymer) substrates. It should be noted that the experimental results showed no qualitative dependence on both the sample thickness and type of the substrate. We found also that the presented technique is not sensitive to the stacking order of graphene layers in multilayer samples. This is in agreement with[27–30] indicating that in the subpicosecond time scale, the intralayer processes dominate the carrier dynamics, while the dynamics at later times is governed by the interlayer coupling.

In order to induce the ultrafast photocurrents in the graphene sample we employed a 1 kHz Ti:Sapphire femtosecond oscillator/amplifier (pulse width 120 fs, central wavelength of 790 nm) and optical parametric oscillator pumped with the fundamental beam (1064 nm) of Nd:YAG laser. The latter system delivers 10 ns pulses at a central wavelength, tunable in the range from 1150 nm to 4000 nm, with 10 Hz repetition rate. In both cases the pump beam was linearly polarized. The polarization plane azimuth varied from p- to s- by a stepwise rotating a half-waveplate positioned before the sample. In all measurements, the pump beam was directed to the graphene sample surface at oblique incidence without any focusing. The incidence angle was controlled with a rotation stage while the excitation beam spot size on the sample was controlled with an iris aperture and varied from 200 μm to 0.5 cm.

To detect the induced photocurrents across the sample we attach to its surface two parallel conductive stripe-line electrodes connected to a 400 MHz digital oscilloscope with 50 Ω input impedance under short-circuit conditions. The typical waveforms of the photocurrent obtained under femtosecond and nanosecond laser pulses incident at 45° in a transversal geometry (the electrodes are perpendicular to the incidence plane of the pump beam, see inset of Fig. 2a) are presented in Fig. 1. The waveforms obtained with a high-speed InGaAs photodiode placed instead of the graphene sample are also shown for comparison. One can see that at the excitation with 10 ns laser pulses, the temporal profiles of the photocurrents induced both in single and ML graphene samples almost coincide with the one obtained from the photodiode. At the excitation with 120 fs pulse,
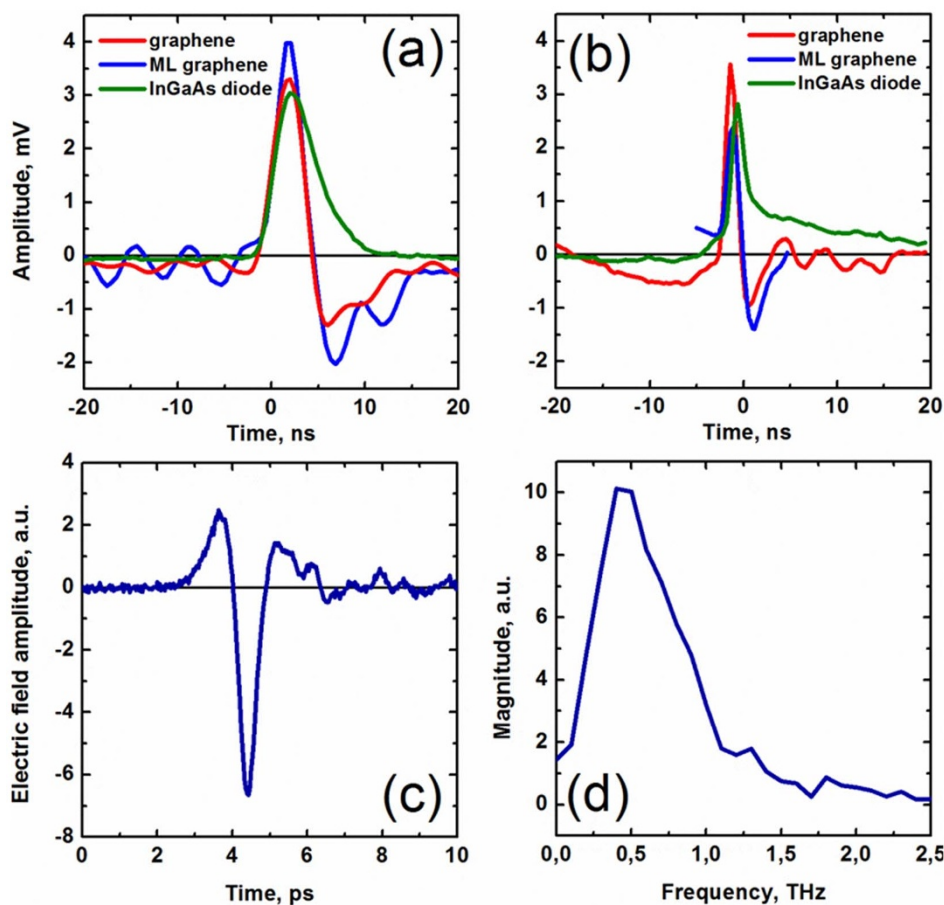
Figure 1 | Waveforms of the photocurrents induced in single layer (red lines) and multilayer graphene (blue lines). The measurements performed in transversal geometry at incidence angle of θ = 45°. (a) The waveform obtained from graphene under excitation with 10 ns pulse (a) and with 120 fs pulse (b). Green lines on figure (a) and (b) represent the response of InGaAs photodiode placed instead of graphene sample. (c) Time-domain waveform of the THz field generated in graphene. (d) Spectrum of the THz signal generated in graphene.
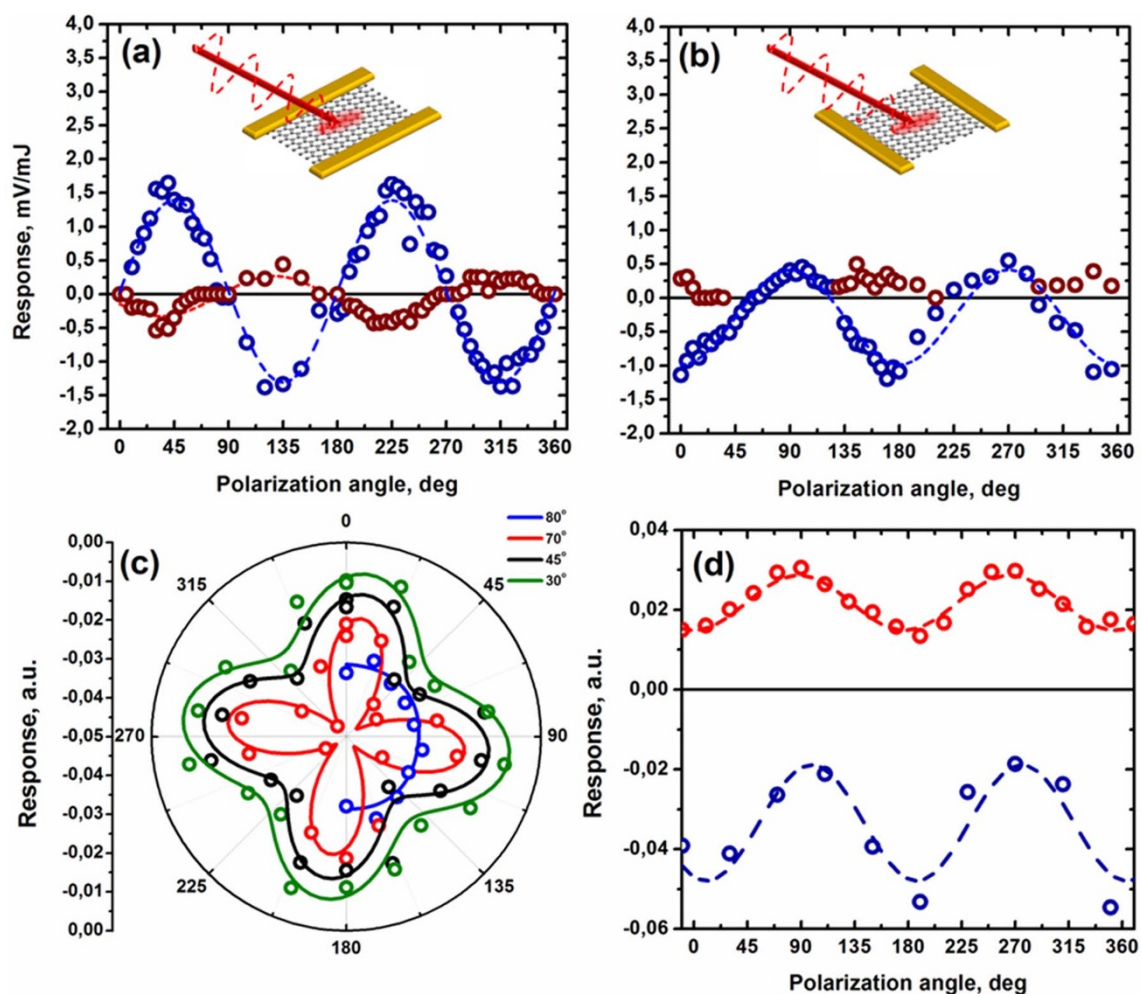
Figure 2 | The polarization dependencies of the photocurrents induced in graphene in longitudinal (a) and transversal (b) experimental geometries, correspondingly, at the incidence angle $\theta = 45°$: Blue points correspond to the photon drag current, red points correspond to other contributions including photogalvanic effect. (c)The induced photon drag current amplitude as a function of the half-waveplate angle measured in the transversal geometry at different incidence angles ($\theta = 80°, 70°, 45°, 30°$). (d) The photon drag current magnitude injected under irradiation from the graphene (blue circles) and substrate side (red circles). Solid and dashed lines on (a–d) are fits to equation (2).

the duration of the signal obtained from graphene samples and the photodiode is determined by the registration system bandwidth, while its magnitude represents the time-integrated current. In the case of the excitation with femtosecond pulses we were also able to detect terahertz (THz) field emitted from the irradiated graphene sample. The observed THz emission expectedly confirmed the ultra-fast origin of the photocurrent induced in graphene. Figures 1(c) and (d) present the measured waveform and spectrum of the THz signal emitted from the contact-free area of the graphene sample. The details of THz emission experiment[31] in graphene are presented in Supplementary information.

The amplitude of the photocurrent was measured in longitudinal (the contacts are parallel to the incidence plane, see inset in Fig. 2(a)) and transversal (the contacts are perpendicular to the incidence plane of the pump beam, see inset in Fig. 2(b)) geometries at different incidence angles and polarization of the excitation beam. We paid special attention to avoid illumination of the contact electrodes and adjacent sample areas, where a built-in electric field exists[32]. The results of these measurements, presented in Fig. 2(c) demonstrate that the magnitude of the induced photocurrent strongly depends on the polarization azimuth (φ) and on the incidence angle (α) of the laser beam at nano- and femtosecond excitation. In both transversal and longitudinal geometries, the photocurrent completely vanishes at normal incidence ($\theta = 0°$) and is maximum at ~45° incidence

angle. At a finite incidence angle, $\theta \neq 0°$, the photocurrent magnitude shows $\sin 2\varphi$- and $\cos 2\varphi$-like behavior in longitudinal and transversal geometries (for details see Supplementary information), respectively (the corresponding fitting curves are shown with solid and dashed lines in Fig. 2). The measured angle and polarization dependencies of the photocurrent resemble those obtained for other nanocarbon materials[18,20].

To demonstrate all-optical control of the transient currents we performed the dual-beam experiment. Since the direction of the photon-drag current is predetermined by the in-plane component of the wavevector of the excitation light wave (see Eq.(2)) we irradiated the front side of the sample with two beams incident at the same angle but the opposite directions (see Fig. 3). While the spectral and temporal parameters of both beams are equal, the polarization azimuth of the first linearly polarized beam is controlled with a half-wave plate. According to the phton-drag theory, in this configuration, each of the beams should induce the in-plane photon drag current of the same magnitude but with the opposite sign, i.e. the laser pulses should produce signals of the opposite polarity.

We first performed the experiment at a zero time delay between the excitation pulses. If the intensities and polarizations of the first and the second beams are equal, the corresponding photocurrents should completely compensate each other resulting in a zero net current and hence a zero potential difference between the electrodes.

In upper part of Fig. 3, one can observe the almost complete compensation of the photocurrent obtained in transversal geometry. The weak nonzero signal (blue lines on Fig. 3(a,b)) is due to a slight difference in the incidence angles and intensities of the two excitation beams. Since the drag current amplitude strongly depends on the polarization of the excitation beam, we were able to tune the net current amplitude by rotating the polarization plane azimuth of the first beam. The net current signal waveforms as a function of the first beam polarization azimuth obtained at nano- and femtosecond excitation are presented in contour plots on Fig. 3 (a) and (b), respectively.
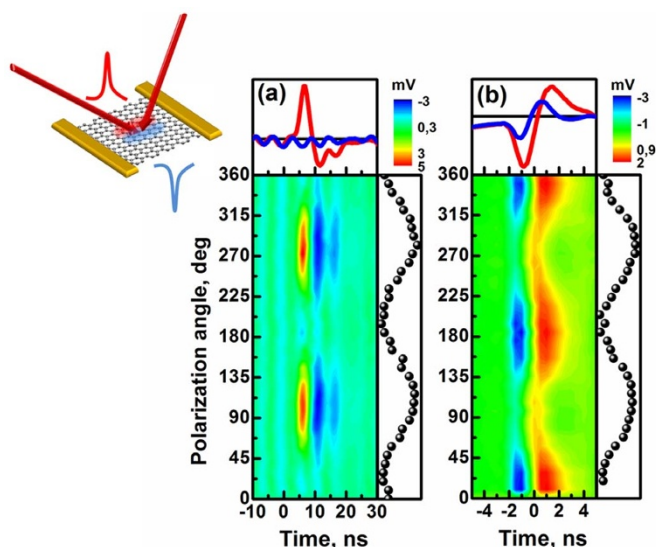
Discussion

The constitutive equation that describes the induced in-plane photocurrent density can be presented in the following form:

$$J_i = \chi_{ijk} E_j E_k^* + \frac{i}{2} T_{ijkl} \left\{ E_j (\nabla_l E_k^*) - (\nabla_l E_j) E_k^* \right\} \quad (1)$$

where E is the complex amplitude of the electric field in the light wave, χ_{ijk} and T_{ijkl} are the material tensors that describe the photogalvanic and photon drag effects, respectively. It is worth noting that although the photogalvanic effect is forbidden in free standing graphene, the presence of the substrate may lift the inversion symmetry giving rise to the current density described by the first term in Eq.(1). The second term in Eq. (1) describes the photon-drag current density, which can be induced in materials of arbitrary symmetry. By taking into account that the six-fold symmetry axis along the graphene normal n reduces the number of independent components of χ_{ijk} and T_{ijkl} down to four and six, respectively, Eq. (1) for the density of in-plane current induced by a linearly polarized beam in graphene yields:

$$J = 2\chi_{xxz} (nE) E^* + T_{xyyx} |[E \times n]|^2 k_{||}$$
$$+ T_{xxyy} (k_{||} E^*) E + T_{xyxy} (k_{||} E) E^* + T_{xzzy} |(En)|^2 k_{||} \quad (2)$$

where $k_{||}$ is an in-plane component of the light wavevector. One can observe from Eq.(2) that the photon drag current changes its direction

with $k_{||}$, i.e. when the graphene sample is irradiated either from the mirror-reflected direction or from the substrate side at the same incidence angle. In contrast, the linear photogalvanic effect contribution to the current remains the same when we irradiate the sample from the opposite side. This gave us an opportunity to identify mechanism responsible for the photocurrent generation obtained in graphene. In the experiment, we observe that switching of the induced photocurrent polarity from positive to negative takes place when graphene is irradiated from the opposite sides (see Fig. 2(d)). This experimental finding clearly indicates that the photon drag effect dominates the photocurrent[33]. The photogalvanic contribution can be identified by occurrence of additional signal with the polarity opposite to the main photon-drag response (negative dips in Fig. 1(a,b) and wine-red circles in Fig. 2(a,b)), which has the same sign for irradiation of the sample from the graphene and the substrate sides.

In order to investigate the interaction between the drag currents we introduce a finite time delay between two 10 ns long excitation pulses. The waveforms of the drag currents induced by each of the beams separately and the corresponding net current waveforms obtained at the different time delays between two pulses are presented in Fig. 4. One can see from Fig. 4 that at the delay time much longer then the pulse width (10 ns), two pulses do not "feel" one another producing signals of the same shape but with the opposite polarity. However, when two pulses temporally overlap, the waveform of the injected current changes. This, in particular, allows one to tune the duration of the net electric signal. It is worth noting that, since the duration of the drag current pulse is only limited by the momentum relaxation time in graphene τ_p, it should be possible to generate the electric signals much shorter than the excitation laser pulse. That is the delay between the laser pulses rather than their duration determines the temporal profile of the net current.
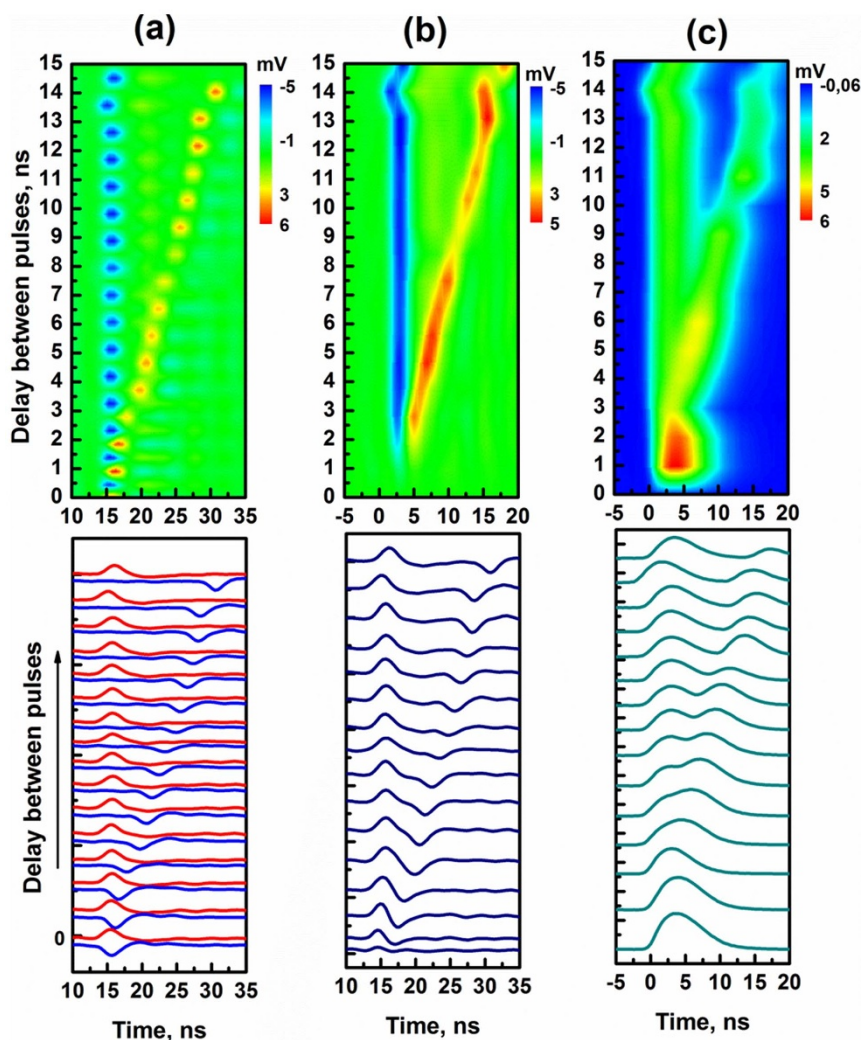
One may expect that the similar effect should be observable, when the opposing components of the net current are induced by two mirrored femtosecond pulses. Although a low bandwidth of our registration system did not allow us to observe the evolution of the net current waveform by changing the time delay between two 120 fs laser pulses, we did observe complete compensation of the time integrated signal produced by the drag currents. This indicates that manipulation of the net current waveform can be also achieved on a pico- or femto- second scale because in graphene the momentum relaxes in the subpicosecond timescale[34]. Such ultrafast currents can be studied via direct detection of the electromagnetic field in THz range emitted during the motion of the dragged carriers. By changing the excitation pulse width and the delay time between the pulses one may manipulate the waveform of the net current and therefore tune the field oscillation frequency in a THz-GHz range. Also this straightforward experiment will elucidate the mechanism of interaction between the carriers simultaneously dragged in the opposite directions.

In conclusion, we proposed and experimentally verified a novel all-optical technique to induce the ultrafast photocurrents in unbiased graphene. The technique is solely based on photon-drag phenomena and provides full and non-contact control of the direction, amplitude as well as temporal profile of the photocurrent in graphene. This opens a very exciting opportunity to generate electromagnetic signals of prescribed waveform utilizing hot carrier dynamics and momentum relaxation in graphene.

Figure 3 | **The contour plots representing the net current waveforms as a function of the first beam polarization state in the dual-beam experiment.** Measurements performed with multilayer graphene sample (~15 atomic layers) on a polymer substrate at zero delay time between pulses. The beams incident at mirror reflection angles in transversal configuration. Excitation with: (a) 10 ns laser pulses centered at 1550 nm, (b) 120 fs laser pulses centered at 790 nm.

Methods

Figure 4 | Upper plates: The waveforms of the photocurrents induced by the two 10 ns pulses incident on the graphene sample at mirror-reflection angles and delayed with respect one another. Red and blue colors correspond to the signals with positive and negative polarity. Lower plates: The waveforms measured at several delay times. (a) The signal measured for each pulse independently when only one of two beams incident onto the sample; (b) The net current obtained when both beams incident on the sample; (c) The signal obtained when both beams incident on the InGaAs photodiode, which was inserted instead of graphene sample.

width 10 ns pulses, central wavelength, tunable in the range from 1150 nm to 4000 nm, 10 Hz repetition rate). The control of polarization was performed by a stepwise rotating a half-waveplate positioned before the graphene sample. The incidence angle was controlled with a rotation stage while the excitation beam spot size on the sample was controlled with an iris aperture and varied from 200 μm to 0.5 cm. The photocurrents induced across the sample were detected with two parallel conductive stripe-line electrodes attached to graphene surface and connected to a 400 MHz digital oscilloscope with 50 Ω input impedance under short-circuit conditions. The details of THz measurements setup are presented in Supplementary information.

1. Novoselov, K. S. *et al.* A roadmap for graphene. *Nature* **490**, 192–200 (2012).
2. Bonaccorso, F., Sun, Z., Hasan, T. & Ferrari, A. C. Graphene photonics and optoelectronics. *Nature Photon.* **4**, 611–622 (2010).
3. Bae, S. *et al.* Roll-to-roll production of 30-inch graphene films for transparent electrodes. *Nature Nano.* **5**, 574–578 (2010).
4. Xia, F., Mueller, T., Lin, Y.-m., Valdes-Garcia, A. & Avouris, P. Ultrafast graphene photodetector. *Nature Nano.* **4**, 839–843 (2009).
5. Sun, D. *et al.* Ultrafast hot-carrier-dominated photocurrent in graphene. *Nature Nano.* **7**, 114–118 (2012).
6. Prechtel, L. *et al.* Time-resolved ultrafast photocurrents and terahertz generation in freely suspended graphene. *Nature Comm.* **3**, 646+ (2012).
7. Sun, D. *et al.* Coherent control of ballistic photocurrents in multilayer epitaxial graphene using quantum interference. *Nano Lett.* **10**, 1293–1296 (2010).
8. Sun, D. *et al.* Evidence for interlayer electronic coupling in multilayer epitaxial graphene from polarization-dependent coherently controlled photocurrent generation. *Phys. Rev. B* **85**, 165427+ (2012).
9. Rioux, J., Burkard, G. & Sipe, J. E. Current injection by coherent one- and two-photon excitation in graphene and its bilayer. *Phys. Rev. B* **83**, 195406+ (2011).
10. Hendry, E., Hale, P. J., Moger, J. J., Savchenko, A. K. & Mikhailov, S. A. Strong nonlinear optical response of graphene flakes measured by four-wave mixing. *Phys. Rev. Lett.* **105** (2009).
11. Mele, E. J., Král, P. & Tománek, D. Coherent control of photocurrents in graphene and carbon nanotubes. *Phys. Rev. B* **61**, 7669–7677 (2000).
12. Danishevskii, A. M., Kastal'skii, A. A., Ryvkin, S. M. & Yaroshetskii, I. D. Dragging of free carriers by photons in direct interband transitions in semiconductors. *Sov. Phys. JETP* **31**, 292–295 (1970).
13. Boiko, I. I. On charge carrier drag by transverse electromagnetic waves. *phys. stat. sol. (b)* **55**, K149–K152 (1973).
14. Grinberg, A. A. & Luryi, S. Theory of the photon-drag effect in a two-dimensional electron gas. *Phys. Rev. B* **38**, 87–96 (1988).
15. Glazov, M. M. Second harmonic generation in graphene. *JETP Lett.* **93**, 366–371 (2011).
16. Bykov, A. Y., Murzina, T. V., Rybin, M. G. & Obraztsova, E. D. Second harmonic generation in multilayer graphene induced by direct electric current. *Phys. Rev. B* **85**, 121413+ (2012).
17. Wu, S. *et al.* Quantum-Enhanced tunable Second-Order optical nonlinearity in bilayer graphene. *Nano Lett.* **12**, 2032–2036 (2012).
18. Obraztsov, A. N. *et al.* Photon drag effect in carbon nanotube yarns. *Appl. Phys. Lett.* **94**, 231112+ (2009).
19. Mikheev, G. M., Zonov, R. G., Obraztsov, A. N. & Yu. Giant optical rectification effect in nanocarbon films. *Appl. Phys. Lett.* **84**, 4854–4856 (2004).
20. Obraztsov, P. A., Mikheev, G. M., Garnov, S. V., Obraztsov, A. N. & Svirko, Y. P. Polarization-sensitive photoresponse of nanographite. *Appl. Phys. Lett.* **98**, 091903+ (2011).

21. McIver, J. W., Hsieh, D., Steinberg, H., Jarillo-Herrero, P. & Gedik, N. Control over topological insulator photocurrents with light polarization. *Nature Nano.* **7**, 96–100 (2011).

22. Entin, M. V., Magarill, L. I. & Shepelyansky, D. L. Theory of resonant photon drag in monolayer graphene. *Phys. Rev. B* **81**, 165441 (2010).

23. Karch, J. *et al.* Photon helicity driven electric currents in graphene, Preprint at http://arxiv.org/pdf/1002.1047 (2010).

24. Jiang, C. *et al.* Helicity-dependent photocurrents in graphene layers excited by mid-infrared radiation of a CO_2 laser. *Phys. Rev. B* **84**, 125429 (2011).

25. Obraztsov, A. N., Obraztsova, E. A., Tyurnina, A. V. & Zolotukhin, A. A. Chemical vapor deposition of thin graphite films of nanometer thickness. *Carbon* **45**, 2017–2021 (2007).

26. Kaplas, T., Zolotukhin, A. & Svirko, Y. Thickness determination of graphene on metal substrate by reflection spectroscopy. *Opt. Express* **19**, 17226–17231 (2011).

27. Carbone, F. *et al.* Femtosecond carrier dynamics in bulk graphite and graphene paper. *Chem. Phys. Lett.* **504**, 37–40 (2011).

28. Breusing, M. *et al.* Ultrafast nonequilibrium carrier dynamics in a single graphene layer. *Phys. Rev. B* **83**, 153410+ (2011).

29. Gilbertson, S. *et al.* Tracing ultrafast separation and coalescence of carrier distributions in graphene with time-resolved photoesmission. *J. Phys. Chem. Lett.* **3**, 64–68 (2012).

30. Obraztsov, P. *et al.* Broadband light-induced absorbance change in multilayer graphene. *Nano Lett.* **11**, 1540–1545 (2011).

31. Won, R. View from... NPO 2010: Bridging the terahertz gap. *Nature Photon.* **4**, 673–674 (2010).

32. Mueller, T., Xia, F. & Avouris, P. Graphene photodetectors for high-speed optical communications. *Nature Photon.* **4**, 297–301 (2010).

33. Ivchenko, E. L. Photoinduced currents in graphene and carbon nanotubes. *Phys. Stat. Solidi B* **249**, 2538–2543 (2012).

34. Hwang, E. H. & Sarma, S. D. Single-particle relaxation time versus transport scattering time in a two-dimensional graphene layer. *Phys. Rev. B* **77**, 195412+ (2008).

Acknowledgments

Author contributions

All experiments were proposed and performed by P.A.O. The CVD graphene samples were provided by T.K. and A.N.O. P.A.O. & Y.P.S. co-wrote the manuscript. Y.P.S. performed the theoretical analysis of the results and supervised the work. K.M.G. provided the THz facility and participated in discussion of the results. S.V.G. and A.N.O. participated in interpretation of the obtained results and gave valuable comments on the paper.

Additional information

Supplementary information accompanies this paper at http://www.nature.com/scientificreports

Competing financial interests: The authors declare no competing financial interests.

How to cite this article: Obraztsov, P.A. *et al.* All-optical control of ultrafast photocurrents in unbiased graphene. *Sci. Rep.* **4**, 4007; DOI:10.1038/srep04007 (2014).